

1 **Sediment structure and physicochemical changes following tidal inundation**
2 **at a large open coast managed realignment site**

3 Jonathan J. Dale^{1,2*}, Andrew B. Cundy³, Kate L. Spencer⁴, Simon J. Carr^{4,5}, Ian W. Croudace³,
4 Heidi M. Burgess¹ and David J. Nash^{1,6}

5 ¹Centre for Aquatic Environments, School of Environment and Technology, University of
6 Brighton, Brighton, BN2 4GJ, UK.

7 ²School of Energy, Construction and Environment, Coventry University, Coventry CV1 5FB,
8 UK.

9 ³School of Ocean and Earth Science, University of Southampton, National Oceanography
10 Centre (Southampton), Southampton, SO14 3ZH, UK.

11 ⁴School of Geography, Queen Mary University of London, London, E1 4NS.

12 ⁵Science, Natural Resources & Outdoor Studies, University of Cumbria, Rydal Road,
13 Ambleside, Cumbria LA22 9BB, U.K.

14 ⁶School of Geography, Archaeology and Environmental Studies, University of the
15 Witwatersrand, Private Bag 3, Wits 2050, South Africa.

16

17 ***Corresponding Author:**

18 Jonathan Dale

19 School of Environment and Technology, University of Brighton, Cockcroft Building, Lewes
20 Road, Brighton, UK, BN2 4GJ. Email: J.J.Dale@brighton.ac.uk

21

22 **Published in *Science of the Total Environment* 660: 1419-1432**

23 **28 December 2018**

24 **DOI: 10.1016/j.scitotenv.2018.12.323.**

25

26 **Authors' version**

27

28 **Keywords**

29 Managed realignment; Microtomography; Sediment Structure; Saltmarsh Geochemistry;

30 Itrax XRF

31

32 **1 Abstract**

33

34 Managed realignment (MR) schemes are being implemented to compensate for the loss of
35 intertidal saltmarsh habitats by breaching flood defences and inundating the formerly
36 defended coastal hinterland. However, studies have shown that MR sites have lower
37 biodiversity than anticipated, which has been linked with anoxia and poor drainage resulting
38 from compaction and the collapse of sediment pore space caused by the site's former
39 terrestrial land use. Despite this proposed link between biodiversity and soil structure, the
40 evolution of the sediment sub-surface following site inundation has rarely been examined,
41 particularly over the early stages of the terrestrial to marine or estuarine transition. This
42 paper presents a novel combination of broad- and intensive-scale analysis of the sub-
43 surface evolution of the Medmerry Managed Realignment Site (West Sussex, UK) in the
44 three years following site inundation. Repeated broad-scale sediment physiochemical
45 datasets are analysed to assess the early changes in the sediment subsurface and the
46 preservation of the former terrestrial surface, comparing four locations of different former
47 land uses. Additionally, for two of these locations, high-intensity 3D-computed X-ray
48 microtomography and Itrax micro-X-ray fluorescence spectrometry analyses are presented.
49 Results provide new data on differences in sediment properties and structure related to the
50 former land use, indicating that increased agricultural activity leads to increased compaction
51 and reduced porosity. The presence of anoxic conditions, indicative of poor hydrological
52 connectivity between the terrestrial and post-inundation intertidal sediment facies, was
53 only detected at one site. This site has experienced the highest rate of accretion over the
54 terrestrial surface (*ca.* 7 cm over 36 months), suggesting that poor drainage is caused by the

55 interaction (or lack of) between sediment facies rather than the former land use. This has
56 significant implications for the design of future MR sites in terms of preparing sites, their
57 anticipated evolution, and the delivery of ecosystem services.

58

59

60 **2 Introduction**

61

62 Saltmarsh and mudflat environments provide a range of ecosystem services (Costanza et al.,
63 1997) including detoxification, nursery habitat and flood defence through the attenuation of
64 wave energy (e.g. Moller et al., 2014; Rupprecht et al., 2017). However, these habitats are
65 threatened by sea level rise, causing erosion and coastal squeeze (e.g. Doody, 2004), and
66 anthropogenic pressures including pollution and reclamation in response to urbanisation
67 and population growth. This has resulted in the loss and degradation of coastal habitats
68 worldwide. In recent years, there have been a number of schemes implemented to
69 compensate for these losses, frequently driven by legislative requirements to improve
70 habitats and biodiversity such as the EU Habitats Directive (European Parliament and the
71 Council of the European Commission, 1992). These schemes use ecological engineering (or
72 ecoengineering) approaches (Bergen et al., 2001) and aim to restore the structure and
73 function of intertidal environments, either through habitat creation or by engineering
74 physical processes to create the desired conditions to encourage habitat creation (Elliott et
75 al., 2016). This paper focuses on managed realignment (MR), one of the most popular
76 coastal ecoengineering techniques.

77

78 MR describes the practice of inundating areas of the coastal hinterland through de-
79 embanking, removing or breaching the former flood defences, with new defences
80 constructed inland. Yet, growing evidence suggests that saltmarshes within MR sites have
81 lower biodiversity and abundance of key species than anticipated (e.g. Mazik et al., 2010;
82 Mossman et al., 2012), which may have consequences for ecosystem functioning (Doherty

83 et al., 2011). These differences have been associated with abiotic factors such as nutrient
84 availability, salinity and redox conditions (Erfanzadeh et al., 2010; Mossman et al., 2012).
85 MR is often carried out in areas of former saltmarsh and mudflat habitat, which have been
86 previously reclaimed through the construction of embankments and then drained for
87 agriculture. As a consequence, the practice results in the restoration and re-creation of
88 historical intertidal habitats (as opposed to creating “new” habitats). Reclamation and
89 drainage leads to compaction, de-watering and mineralisation of organic matter, resulting in
90 irreversible changes to the sub-surface sediment structure (including the collapse of pore
91 space) (e.g. Crooks and Pye, 2000; Hazelden and Boorman, 2001; Spencer et al., 2017). This
92 has led to poor drainage in many MR sites following site inundation and reduced vertical
93 hydrological connectivity between the relict terrestrial horizon and the freshly deposited
94 intertidal sediment (e.g. Crooks and Pye, 2000; Hazelden and Boorman, 2001; Tempest et
95 al., 2015).

96

97 The flux of pore water through the sub-surface sediment is considered to be crucial for
98 controlling abiotic conditions, and therefore could exert a major influence on vegetation
99 colonisation in MR sites (Davy et al., 2011; e.g. Howe et al., 2010; Wilson et al., 2015).

100 However, there remains a shortage of data on the evolution of sub-surface sediment
101 geotechnical and geochemical properties following inundation at MR sites (Esteves, 2013).
102 This is especially true for investigations into the critical period immediately following site
103 inundation (i.e. in the early stages of the terrestrial to marine or estuarine transition) as it is
104 these surface conditions that will form the substrate for seedling germination, with
105 particular focus required into:

- 106 (a) the preservation of the relict terrestrial horizon, and its structural, physical and
107 chemical characteristics, post-inundation, and
- 108 (b) the development of the sub-surface geochemical profile in response to the former
109 terrestrial land use.

110

111 This study investigates the impact of different pre-managed realignment land use practices
112 on the early evolution of the sub-surface sediment structure and geochemical environment
113 at the Medmerry Managed Realignment Site (West Sussex, UK), during the first three years
114 of site inundation (covering the early stages of the transition from a terrestrial to a marine /
115 coastal lagoonal system). Specifically, a novel combination of broad- (centimetre to
116 decimetre) and intensive- (micron) scale sedimentary data sets, from samples taken at two
117 time points, are analysed to assess the differences and the early evolution of the sub-
118 surface geochemical profile and sediment structure for sites of differing former land use.
119 The implications of these differences for the longer term development of sediment
120 structure, drainage and physicochemical properties, in relation to site evolution,
121 management, and ecosystem service delivery, are discussed and assessed.

122

123 **3 Study Site**

124

125 The Medmerry Managed Realignment Site (Figure 1) is located within the Solent, southern
126 UK, on the western side of the Manhood Peninsula (Figure 1, insert). Previously, the area

127 had been a brackish lagoon (Krawiec, 2017) behind a shingle barrier beach, which had
128 drained through Pagham Harbour on the eastern side of the peninsula. However, this area
129 was separated from Pagham Harbour and reclaimed through the construction of an
130 embankment, and subsequently drained, between 1805 and 1809 (Bone, 1996). Coastal
131 flood defence for the reclaimed area at Medmerry was provided by the shingle barrier
132 beach, which was managed by the Environment Agency (UK). To maintain the necessary
133 defence standard, constant work was required each winter to recycle and re-profile the
134 shingle bank. Nevertheless, the defences remained vulnerable during storm events; the
135 bank was breached 14 times between 1994 and 2011, flooding homes, local holiday caravan
136 parks and agricultural land. The coastal flooding and erosion risk was reviewed in the
137 Pagham to East Head Coastal Defence Strategy (Environment Agency, 2007), which
138 endorsed MR as the most suitable method of managing the risk of coastal flooding.

139

140 The Medmerry scheme, which is the largest open coast MR site in Europe (at the time of site
141 inundation), was designed not only to provide a sustainable and cost-effective method of
142 coastal flood risk management, but also to compensate for saltmarsh and mudflat habitat
143 loss elsewhere in the region. Over 80% of the Solent's coastline is designated for its nature
144 conservation interest (Foster et al., 2014), yet 40% (approximately 670 hectares) of
145 saltmarsh in the region were lost through erosion between 1971 and 2001 (Cope et al.,
146 2008). Over the one hundred years following construction of the Medmerry site, it was
147 estimated that up to 184 hectares of new intertidal and transitional habitat would be
148 created (Pearce et al., 2011).

149

150 Construction of the site began in autumn 2011, which included 7 km of new earth “bund”
151 defences, reaching 3 km inland. Freshwater drains through the site via four drainage outlets
152 with tidal gates constructed into the new defences. The site was breached on 9th
153 September 2013 through a single narrow opening in the shingle bank, forming a semi-
154 diurnal, mesotidal, semi-enclosed, fetch and depth limited estuarine system. At the time of
155 this study, high water at the furthest point inland occurred approximately 50 minutes after
156 high water at the breach (Dale et al., 2018b). During low tide, draining water is constricted
157 to the main channels running through the site (Figure 1), which in some cases drain to near
158 emptiness. Sediment is imported, and exported, from the wider coastal environment, but
159 Dale et al. (2018b) identified that larger concentrations are currently being internally
160 redistributed as the site responds to the introduction of intertidal inundation.

161

162 **4 Materials and Methods**

163

164 Six sediment cores were taken from the Medmerry site in each of 2015 and 2016. All
165 sampling was performed at low water. Cores 1 to 4 were collected for broad-scale analysis,
166 Cores 5 and 6 for intensive-scale analysis. Sampling was carried out at four locations within
167 the Medmerry site. These locations were selected based on differences in former
168 (terrestrial) land use. Cores 1 and 5 were taken from a former area of pastoral land,
169 occasionally used for low quality (usually unsuccessful) arable agriculture. Cores 2 and 3
170 were from a former area of pastoral land, with Core 2 taken from a non-vegetated surface
171 and Core 3 from a vegetated surface. Cores 4 and 5 were from a former intensive arable
172 field, last harvested two weeks prior to site inundation, behind an area of lower elevation
173 land which has experienced rapid accretion of coarse grained sandy sediment ($d_{50} = 47.33 \pm$
174 $0.91 \mu\text{m}$) following site inundation (Dale et al., 2017). The expected differences in sediment
175 structure as a result of the former land use are outlined in Table 1. The presence and extent
176 of these proposed differences were assessed initially on a broad centimetre scale, followed
177 by analysis carried out on an intensive (micron) scale.

178

179 **4.1 Sampling and Methods for Broad (centimetre to decimetre)-Scale Analysis**

180

181 Vertical sediment cores were taken in January 2015, 16 months after the site was breached,
182 and September 2016, 36 months after site inundation, to evaluate differences in the
183 sediment sub-surface physical properties and geochemistry. Two cores were taken in

184 parallel, at approximately the same elevation (± 2 cm) and within 30 cm of each other, at
185 each sampling location using a hand driven large (5cm diameter, stainless steel) gouge
186 corer, transferred to open PVC tubes and wrapped in PVC film. Due to topographic
187 variations within the site it was not possible to sample at identical elevations at the four
188 sampling sites, but all sites were approximately in the same position in the intertidal zone
189 and therefore are expected to have similar hydroperiod conditions. Core depths varied
190 between 26 and 49 cm, although parallel cores were not always taken to the same depth.
191 Sediment cores were collected at least 15 m from the channel to minimise the influence of
192 lateral sub-surface flow (Marani et al., 2006).

193

194 Samples were stored at + 3.6 °C until analysis. Sediment properties were visually described
195 and one core from each site was subsampled at 1 cm depth increments. Following hydrogen
196 peroxide treatment and dispersion with sodium hexametaphosphate, a Malvern
197 Instruments Mastersizer Hydro 2000G Laser Diffraction Particle Size Analyser was used to
198 determine the grain size distribution in sediment subsamples. Subsamples were also
199 examined for a suite of elements using an Inductively Coupled Plasma-Optical Emission
200 Spectrometer (ICP-OES). Samples were digested with Aqua Regia (modified from Berrow
201 and Stein, 1983). Aqua Regia was prepared with a 30% HNO₃ : 70% HCL (1:3) mixture at
202 room temperature. 0.1 ± 0.01 g of sample, oven dried at 105 °C, was digested in 3 ml of
203 Aqua Regia for three hours in a water bath at 80 °C. Following digestion, 7 ml of distilled
204 water were then added to the sample. A 1:10 dilution of the solution was made with
205 distilled water for analysis using a Perkin Elmer Optima 2100 DV ICP-OES. To assess the
206 elemental recovery of the digestion procedure the measured values were compared to the

207 quoted values for a Certified Reference Material (CRM) digested and analysed alongside the
208 samples (e.g. Cochran et al., 1998). The Mess-4 Marine Sediment (National Research Council
209 Canada) CRM was used and recovery values were generally within $\pm 25\%$ of the reported
210 values (see supporting information). Process blanks and repeat samples were analysed
211 every 20 samples for quality control and analytical error. Process blanks were below
212 detection limits and repeat samples were within $\pm 10\%$ throughout.

213

214 For the remaining cores, a known quantity of sediment was extracted using a syringe at 1
215 cm intervals and analysed for wet bulk density, moisture content, porosity and loss on
216 ignition (a proxy for organic content). The moisture content was measured as a percentage
217 of the dry mass (moisture content = water weight / dry sediment weight x 100) after
218 samples had been oven dried at 105 °C for 48 hours. Porosity was calculated using the dry
219 bulk density, assuming a particle density of 2.65 g cm⁻³ as stated by (Rowell, 1994) based on
220 typical data. The organic content of the samples was estimated via the loss on ignition proxy
221 method, following ignition of subsamples for six hours at 450 °C.

222

223 **4.2 Sampling and Methods for Intensive (micron)-Scale Analysis**

224

225 Smaller sediment cores were recovered from the same coring locations as Core 1 and Core
226 4, labelled Cores 5 and 6 respectively, in July 2015 and September 2016. These sites were
227 selected to analyse the influence that different intensities of arable agricultural activity have
228 on the subsurface sediment structure (i.e. by using sites with / without a history of intensive

229 arable agriculture). Cores were taken from within 2 m of the broad-scale coring sites, using
230 the advanced trimming method (Hvorslev, 1949). 44 mm diameter clear PVC tubes were
231 inserted into the sediment, trimming the surrounding sediment to minimise the disturbance
232 to the sample. Core lengths varied between 7.9 cm and 11.1 cm. The ends of the sample
233 tubes were capped and wrapped in PVC film secured with tape to prevent moisture loss.
234 Cores were kept upright during transport and storage to minimise any disturbance and, on
235 return to the laboratory, were stored between + 3.6 °C and + 4 °C.

236

237 3D-computed X-ray microtomography (μ CT) is a non-destructive imaging method that has
238 been successfully applied to the study of saltmarsh sediment structure (Cnudde and Boone,
239 2013; Ketcham and Carlson, 2001; Spencer et al., 2017). μ CT analysis was carried out here to
240 identify the sediment bulk phases and stratigraphy (for an assessment of the comparability
241 of the broad- and intensive-scale methodologies) and to analyse the key structural and
242 stratigraphic differences (total porosity, characterisation of the pore networks) between the
243 two sampled sites, at a much higher resolution than the broad-scale approach described
244 above. Whilst only single core samples were analysed in both years per core site, previous
245 analysis of this type (e.g. Spencer et al., 2017) has recognised that single core samples may
246 be used as a representation of the sediment structural characteristics. Sealed core tubes
247 were scanned at 76 μ m resolution using a Nikon Metrology XT H 225 X-ray CT system with
248 Perkin Elmer XRD 0820 CN3 16-bit flat panel detector at Queen Mary, University of London.
249 Inspect-X was used to perform the scans and X-radiogram acquisition and reconstruction
250 was undertaken in CTPro. Drishti 2.1 volume rendering software was used for visualisation
251 of the reconstructed 3D models to identify bulk phases and inform segmentation following

252 the method of Spencer et al. (2017). Each 3D volume was sub-sampled further into four
253 equally sized depth increments, labelled A (base) to D (top), for detailed quantification of
254 differences in porosity with depth.

255

256 Cores were split vertically, photographed and analysed using Itrax non-destructive micro-X-
257 ray fluorescence spectrometry analysis (Croudace et al., 2006) for a range of elemental data
258 to compare changes in geochemistry with sediment structure analysis provided by the μ CT,
259 at a 200 micrometre scale which was not possible using ICP-OES analysis. The Itrax produces
260 elemental data in counts but previous studies (e.g. Miller et al., 2014) have shown that
261 these data correlate well with quantitative analytical data (e.g., ICP-OES or Wavelength
262 Dispersive X-ray Fluorescence). Furthermore, the high frequency compositional changes
263 identified using the Itrax are often missed when analysing lower resolution bulk sub-
264 samples using more traditional, destructive, analytical methods. Each core was loaded onto
265 a horizontal cradle and scanned at a resolution of 200 μ m at the BOSCORF laboratories,
266 National Oceanography Centre (Southampton). Cores were scanned wet to preserve
267 internal structure, with the software correcting for water content. Core Scanner Navigator
268 software was used to control the scanner, and data were plotted and displayed using Q-
269 Spec software. The Itrax scanner combines an X-ray line camera with a narrow, parallel,
270 high-flux X-ray beam to record a radiograph at 55 kV. XRF analysis was performed at 30 kV
271 (using a Mo anode X-ray tube, counting time 30s). Data were plotted using ItraX-Plot,
272 described by Croudace et al. (2006).

273

274 **5 Results**

275

276 **5.1 Broad-scale (centimetre to decimetre) Physicochemical Changes in the** 277 **Subsurface (Cores 1 to 4, 2015 and 2016)**

278

279 Sediment cores 1 to 4 exhibited clear vertical zonation and could be divided into three facies
280 (from core base to core surface) based on the environmental and land use change known to
281 have occurred at the Medmerry site; (i) a pre-reclamation intertidal unit (*Unit A*), (ii) a
282 reclamation boundary and soil unit formed since site reclamation between 1810 and 1880
283 (*Unit B*), and (iii) a terrestrial boundary and post-breach intertidal unit dating from site
284 inundation in September 2013 (*Unit C*). The depth, composition and structure of the three
285 units varied between sites.

286

287 **5.1.1 Physical Characteristics**

288

289 Average physical sediment characteristics for the three units are presented in Table 2 (see
290 supplementary material for core descriptions and full datasets). Wet bulk density ranged
291 from 0.64 to 2.18 kg m⁻³ and tended to increase with depth. Both moisture content (36.62 –
292 123.08 %) and porosity (0.33 – 0.81) decreased with depth, whereas loss on ignition values
293 varied from 3.24% to 19.21% and fluctuated through the sample. Coarser grained sediments
294 were generally found in the Unit A, compared to Units B and C, except in Core 4 where
295 coarser grained sediments ($d_{50} = 67.87$ (2015) and 49.77 (2016)) were found at the sediment

296 surface. Median grain sizes ranged from 5.46 to 46.48 μm , and the mud content (clay + silt)
297 varied between 54.1 and 97.67 %. Statistical differences between sediment units were
298 assessed via a Kruskal Wallis test ($n = 22$ to 45 , $p < 0.05$) for the whole dataset with the
299 exception of Core 4₁₆ as no vertical zonation was found in this sample. Statistical differences
300 were found between the three sediment units for all parameters except for particle size
301 analysis (median grain size and mud content).

302

303 **5.1.2 Geochemical Profiles**

304

305 ICP-OES-derived major element data (Al, Ca, Fe, Mn, S, Na) are presented for 2015 (Figure 2)
306 and 2016 samples (Figure 3). To account for variations in sediment composition, data have
307 been normalised to Al (after Spencer et al., 2008). Ca decreased with depth through Unit C
308 in all 2015 samples and Cores 2 and 3 in 2016. This may be the result of decalcification,
309 typical of oxic saltmarsh sediments as a result of a lowering of the pH caused by nitrification
310 and decomposition of organic matter (Luther and Church, 1988; Vranken et al., 1990), and
311 then re-precipitation at depth. However, the scale of the decrease, and subsequent increase
312 in Unit A (Core 1₁₅ and Core 4₁₅) could also be indicative of the presence of finely
313 comminuted shell debris in the intertidal sediments (Units A and C).

314

315 The diagenetic cycles of Fe and Mn have been well documented for saltmarsh sediments
316 (e.g. Spencer et al., 2003; Zwolsman et al., 1993). A peak in Fe or Mn concentration may
317 indicate redox mobilisation and reprecipitation, whereas an increase in S may represent

318 bacterially-mediated reduction of sulphate and formation of early-diagenetic sulphide
319 minerals (Cundy and Croudace, 1995). In both years at coring locations 1, 2 and 4, and in
320 Core 3₁₅, Fe and Mn concentrations were relatively homogenous down core with some
321 variability within Unit B, potentially caused by residual Fe concretions from the legacy of
322 ploughing within this zone, without any consistent or clear peaks. This is suggestive of a
323 fluctuating water table through the sediment sub-surface, consistent with the visual
324 observations of Fe-stained mottled sediment in this zone (see supplementary material); this
325 may be the result of tidal variability causing changes in the redox boundary, preventing the
326 formation of a stable redox zone and a strong Fe and Mn peak (Cundy and Croudace, 1995;
327 Zwolsman et al., 1993). However, in Core 3₁₆, Fe fluctuated throughout the depths
328 examined, peaking in the middle terrestrial zone. A clearer trend was observed in the
329 concentration of Mn, which is more sensitive than Fe to changes in redox status, with Mn
330 peaking at the boundary between the post-breach intertidal and terrestrial facies suggesting
331 possible diagenetic enrichment of Mn. S concentration decreased with depth, matching the
332 changes in Na concentration, and therefore implying that variations in S are driven primarily
333 by the introduction and evaporation of sea water.

334

335 Principal component analysis (PCA) was performed on the entire dataset to differentiate
336 between the physical and geochemical characteristics of the different units. PCA is a data
337 reduction technique which calculates new variables, or principal components, from linear
338 combinations of the original parameters and has been used successfully elsewhere to
339 (partially) discriminate geochemical data in coastal sediments (e.g. Cundy et al., 2006). The
340 first principal component accounts for the greatest variability, with every subsequent

341 component accounting for less of the variability (Reid and Spencer, 2009). Therefore, PCA
342 allows for grouping of different depths based on their physicochemical variability. Results
343 reveal clear differences between the PCA scores for Units A and C (Figure 4). Unit B also
344 demonstrated some evidence of grouping, but overlapped the other two units.

345

346 **5.2 Intensive-scale (micron) Subsurface Structure Physicochemical Characteristics**

347

348 **5.2.1 Sediment Structure**

349

350 Representative μ CT reconstructions of sediment structure, with a voxel size of 65 μ m, are
351 presented for coring locations 5 (taken from an area of former lower intensity arable
352 agriculture) and 6 (an area of former high intensity arable agriculture) in Figure 5. Core 5
353 demonstrated a relatively consistent solid matrix phase (Figure 5a) in both years sampled,
354 with no separate sediment facies, suggesting there has been no (or very minimal) post-site
355 inundation deposition of sediment. This is despite the broad-scale geophysical analysis
356 suggesting that a small, 2 cm, new intertidal sediment unit was present. It is, therefore,
357 possible that these different units might be present, but that they are sufficiently similar in
358 sediment structure to be indistinguishable via μ CT analysis. In contrast, structural
359 differences were clearly visible in Core 6₁₅ (Figure 5b). Laminations were present in a
360 compact upper sediment facies, consisting of sandy sediment deposited following site
361 inundation, overlying the former terrestrial soil that had been used intensively for arable
362 agriculture up to two weeks prior to site inundation. A sharp, irregular boundary occurred
363 between the two units and is marked on Figure 5b. No evidence of the upper sediment

364 facies was found in the Core 6₁₆ sample (Figure 5b), probably due to the local remobilisation
365 of sediment in response to observed changes in the site's hydrodynamics, and
366 morphological evolution in response to the introduction to intertidal inundation (Dale et al.,
367 2018a).

368

369 Macroporosity (pores > 80 µm; Beven and Germann, 2013) measurements and
370 characteristics are presented in Table 3, and plotted for each of the four sub-samples in
371 Figure 6. In Core 5₁₅, a large, interconnected, pore space was detected through the sample,
372 whereas the Core 5₁₆ pore structure consisted of horizontal elongated macropore networks.
373 In Core 6₁₅, a sheet like macro-pore was detected across the division between the units,
374 although it is likely that this an artificial feature caused by the coring process (which
375 resulted in sediment cracking along this interface), with a large horizontal macropore
376 dominating the lower facies. There was also no evidence of this horizontal pore system in
377 Core 6₁₆, with the macropore network dominated by a vertical pore (on the left of the 2016
378 macro-pore phase in Figure 5b) and areas of isolated, flattened pore space.

379

380 Bulk macroporosity in Core 5 was generally moderate to high (5.6 – 22.4 %) and decreased
381 with depth (Figure 6), as would be expected due to sediment compaction effects. Less
382 variability was observed in Core 6, where bulk macroposity was low to moderate (3.5 – 13.1
383 %). The degree of pore connectivity is indicated by the Euler-Poincaré characteristic, a
384 measure of the number of redundant connections within the pore network expressed as a
385 function of the volume, with decreased connectivity indicated by increased positive values,

386 and increased connectivity demonstrated by decreased negative values (Vogel, 1997). All
387 samples followed a trend of decreasing connectivity upwards, and then increasing in the
388 upper sub-sample, reflecting an increase in redundant connections and more tortuous pore
389 networks in the upper and lower sediment sub-sections. Connectivity was greater in 2015
390 compared to 2016 at both sites and was greater in Core 5 compared to Core 6, suggesting
391 greater levels of compaction due to higher levels of agricultural activity and an increase in
392 compaction at both sites as each evolved following site inundation.

393

394 The mean number of branches per pore were calculated through the transformation of
395 macropores into topological networks of nodes and branches, and used as an indication of
396 pore network complexity (Polder et al., 2010). Pore networks were more complex in Core 6
397 than Core 5, but at both sites decreased in complexity between 2015 and 2016. This
398 suggests that pore system complexity decreases over time following site inundation, due to
399 either the hydraulic head of tidal water above the sediment causing compaction or
400 sediment being flushed out as the water drains causing the pore networks to collapse (Dale
401 et al., 2018a). No distinct pattern was present in the Core 5₁₅, but in Core 5₁₆ the upper sub-
402 sample had a greater number of branches per pore compared to the rest of the sample. In
403 contrast, complexity in Core 6 decreased upwards, but increased in the upper sub-section
404 consisting of the post-breach sediment facies. The degree of anisotropy is representative of
405 similarity in arrangement and the directness of the branches of the dominant macropore
406 system (Odgaard, 1997). In 2015, pores were more aligned in Core 5 than Core 6, although
407 anisotropy was much lower in the basal sub-samples of Core 5 (A and B). Anisotropy was
408 higher in the post-breach sediment facies in Core 6₁₅. In comparison, macropores

409 demonstrated a similar level of organisation in Core 5₁₆, whereas Core 6₁₆ had a higher
410 anisotropy value representing an increase in similarity in the arrangement of the pore
411 networks.

412

413 **5.2.2 Sediment Geochemistry**

414

415 Itrax scanning was employed to examine the variability of nine elements at high spatial
416 resolution (200 µm). The content of coarse grained sediment, indicated by the Zr and Cr
417 intensity (which are frequently associated with heavy mineral assemblages in detrital sands,
418 e.g. Cundy et al., 2006), remained relatively constant in Core 5₁₅ (Figure 7a). Two major
419 peaks were observed in the Cr intensity, although the second of these peaks corresponded
420 with an area of high intensity present on the radiograph likely to be a clast. Measurements
421 of the K intensity indicate that the fine grained fraction decreased in the middle section of
422 the sample, increasing again deeper in the sample, which is also reflected in Si and the bulk
423 µCT attenuation measurements (Figure 5a). Similar trends were observed in the Cl and Ca
424 intensity. Black sediment, low Fe and Mn, and a peak in S, suggest possible bacterial
425 reduction of sulphate within the cracked and desiccated near-surface sediments (Figure 5a),
426 although broadly coincident peaks in Cl and Ca may indicate that the peak in S is at least
427 partly a function of increased porewater sulphate rather than sulphate reduction processes.
428 Fe and Mn increased below this unit and remained constant throughout the rest of the
429 sample, with three relatively large peaks. However, the Fe peaks corresponded with peaks
430 in X-ray intensity (kcps) and are likely to be the product of X-ray response rather than

431 increases in concentration. After peaking in the near-surface sediment, S followed a similar
432 pattern to Si, K, Cl and Ca.

433

434 No major vertical changes in bulk sediment composition were detected in Core 5₁₆ (Figure
435 7b), demonstrated by the relatively constant distribution of Si with the major peaks
436 corresponding to variability in the X-ray response (kcps). These observations were
437 supported by similar trends in Zr and Cr intensities, although peaks were also observed in
438 these elements corresponding to the presence of high density material (clasts, evident in
439 the X-radiograph image). The distribution of K indicated relatively constant clay content
440 within the sample. Cl decreased slightly down-sample, whereas Ca decreased in the lower
441 section of the sample, indicative of decalcification. In contrast to the other elements, Mn
442 showed a strong increase in intensity in the middle part of the core, possibly reflecting early
443 diagenetic enrichment, although this observation was not supported by change in the Fe
444 intensity. However, analysis of the Fe / Mn ratio (Figure 8) indicated higher concentrations
445 of Mn to Fe in the middle of the core, suggesting mildly reducing conditions and early
446 diagenetic mobilisation of Mn. No evidence of the bacterial reduction of sulphate, possibly
447 present in the near-surface of the previous sample, was found, and trends in S generally
448 coincided with peaks in Cl and Ca so may be caused by increased porewater sulphate rather
449 than microbially-mediated sulphate reduction.

450

451 Coarse grained sediments dominated the near-surface component of Core 6₁₆ (Figure 7c),
452 visible in the photographic image and indicated by the high intensity of Zr. Several peaks in

453 Cr were detected in the upper part of the core, likely to correspond to the laminations
454 observed in the μ CT scan (Figure 5b). At the boundary between the post-breach and
455 terrestrial sediment facies Cr peaked below a unit of low density detected by the
456 radiograph, matching the sheet-like pore space present in the μ CT scan (Figure 5b). Below
457 this unconformity, K intensity increased, and Zr / Cr decreased, indicating an increase in fine
458 grained sediment. Cl generally decreased through the sample, whereas Ca decreased and
459 then increased again. Evidence of sub-surface diagenetic enrichment of Mn was provided by
460 an increase, and peak, in intensity in the lower third of the core. The peak in Mn
461 corresponded to an area of low density measured by the radiograph, although this is not
462 visible on the photography. It is possible that this area is the large horizontal macro-pore
463 feature present in the μ CT analysis. The concentration of Fe also increased through the
464 sample, with areas of enrichment corresponding to red mottling on the sample. The Fe / Mn
465 ratio decreased through the upper 2 cm of the sample (Figure 8), but increased again at a
466 similar depth to the large horizontal macro-pore. Below the terrestrial boundary, S intensity
467 decreased through the sample. Small scale increases in S intensity occurred in areas where
468 red mottling of the sediment was not present.

469

470 In Core 6₁₆ (Figure 7d) coarser grained sediments were only found in the surface sediment,
471 indicated by the surface peak in Zr, consistent with the findings from the broad-scale and
472 μ CT analysis. Trends in K suggested increased clay content was present in the middle of the
473 sample. A peak in Cl occurred within the upper sub-surface, corresponding to a peak in S,
474 which could indicate the depth of saline intrusion into the sediment. Fe and Mn decreased
475 through the top of the red mottled surface sediment. Fe, and to a lesser extent Mn,

476 increased through the middle of the sample, supporting visual observations of red mottling,
477 with an additional increase present in the deeper parts of the sample.

478

479 **6 Discussion**

480

481 **6.1 Preservation of the Pre-Breach Terrestrial Surface**

482

483 Observations made at other, older, MR sites suggest that visual changes in the sediment
484 characteristics associated with a terrestrial boundary or horizon would no longer be present
485 after a number of years. For example, no visual evidence of a terrestrial facies was found at
486 Orplands Farm Managed Realignment Site 8 years after site inundation (Spencer et al.,
487 2008), although at this site a terrestrial horizon could still be detected through analysis of
488 physicochemical properties of the sediment. Broad-scale analysis from four locations at the
489 Medmerry Managed Realignment Site provided visual evidence that a sub-surface
490 unconformity could still be detected at all sites except for Core 4₁₆, the nearest site to the
491 breach (in a significantly higher energy environment than the other sites sampled).
492 However, no uniform stratigraphic marker of the terrestrial surface such as the organic rich
493 peaty horizon identified at Pagham Harbour by Cundy et al. (2002) or the alternating peat-
494 mud (i.e. terrestrial – marine) couplets used elsewhere as indicators of tectonic activity and
495 sea level change in coastal and near-coastal sediments (e.g. Shennan et al., 1996; Shennan
496 et al., 1998) was found, although these have been suggested to be inconsistently preserved
497 in some suddenly submerged intertidal environments (Cundy et al., 2000). In each sample
498 where a sub-surface unconformity was detected, a lower pre-reclamation sediment facies
499 was also detected. PCA allowed (partial) discrimination of samples based on combined
500 physical and geochemical sediment properties, as opposed to a single indicator such as loss

501 on ignition or changes in particle size, into groups which corresponded to one of the three
502 vertical sediment facies; post-breach, terrestrial or pre-reclamation sediments.

503

504 The reclamation of saltmarshes results in modification to sediment structure and properties
505 (e.g. Crooks et al., 2002; Hazelden and Boorman, 2001) as a result of de-watering and
506 organic matter mineralisation, decreasing the porosity and increasing the bulk density. After
507 the re-introduction of intertidal conditions through MR, the legacy of these changes can still
508 be detected, with low moisture contents still being found at depth several decades after site
509 inundation (Spencer et al., 2017). Analysis of sites of different former land use at Medmerry,
510 16 months after site inundation, indicated similar bulk densities and porosities within the
511 terrestrial facies regardless of former site activity and land use. However, moisture content
512 and loss on ignition were higher in Cores 2 and 3, areas which previously had not been
513 subjected to arable agricultural practices (i.e. ploughing).

514

515 Detailed examination of the 3D sediment structure through the use of μ CT allowed
516 comparisons of the morphology and connectivity of the sediment macro-porosity at
517 different coring locations to be made. In Core 5, taken from a site that was previously used
518 occasionally (and usually unsuccessfully) for agriculture, no new intertidal sediment unit was
519 detected despite evidence of separate units in the broad-scale analysis. It is possible that
520 differences observed in the broad-scale analysis are the result of the terrestrial unit
521 transitioning into an intertidal sedimentary environment, rather than consisting of sediment
522 deposited following site inundation. This is reflected in the similarity in the matrix of the

523 sediment detected by the μ CT analysis and the gradual transition between the units
524 observed in Core 1₁₆. Core 5 had a greater bulk macroporosity throughout the sediment
525 sub-surface, with simpler pore networks that were more connected and had greater
526 similarity in arrangement than Core 6, which had been used consistently for high intensity
527 agricultural activity. This indicates that, as a result of the legacy of different terrestrial
528 agriculture practices, different sub-surface structures exist in terms of sediment
529 macroporosity, which is likely to affect the drainage characteristics and therefore
530 geochemical profiles within the sediment subsurface. Terrestrial and post-breach facies
531 were detected in the 2015 3D sediment structural analysis performed on Core 6. The top
532 facies consisted of laminated sediment deposits, which had accreted post-site inundation.
533 When re-sampled, only one sediment facies was detected. This is potentially the result of
534 local remobilisation of intertidal sediment deposited post-site inundation, likely to be in
535 response to changes in site hydrodynamics and morphological evolution as the realignment
536 site evolves.

537

538 Analysis of physical characteristics and structure of the sediment at Medmerry indicate
539 differences in sediment composition, properties and macroporosity for sites of differing
540 former land use, with the terrestrial soil unit still detectable visibly at some sites up to three
541 years after site inundation. These differences may well have consequences for the
542 development of geochemical profiles, which might limit the colonisation of saltmarsh
543 vegetation (Davy et al., 2011) and explain the lower biodiversity and abundance of key
544 species observed elsewhere (e.g. Mazik et al., 2010; Mossman et al., 2012). Importantly,
545 however, levels of sediment accretion over the terrestrial unit were much lower than at

546 other older sites (typically 20 to 40 mm at Medmerry compared to, for example, *ca.* 60 mm
547 at Orplands Farm) (Spencer et al., 2008), which may partly mitigate any discontinuities in
548 hydrological connectivity caused by the deposition of intertidal sediment on top of the
549 preserved terrestrial surface.

550

551 **6.2 Implications for Geochemical Profile Development at Managed Realignment** 552 **sites**

553

554 Typical vertical saltmarsh geochemical profiles are controlled by strong physicochemical
555 gradients in pH and redox potential, and microbially-mediated organic matter breakdown
556 using electron acceptors such as O₂, MnO₂ and Fe(OH)₃ (e.g. Koretsky et al., 2005; Spencer
557 et al., 2003). Following reclamation and ploughing large-scale precipitation of Fe
558 oxyhydroxides and other Fe-rich minerals would be anticipated (Auxtero et al., 1991;
559 Violante et al., 2003). When re-introduced to intertidal conditions remobilisation of Fe by
560 the saline water is expected through dissimilatory reduction of sulphate or dissolved Fe
561 being re-distributed by advection caused by the local hydrology (Burton et al., 2011;
562 Johnston et al., 2011). However, impeded vertical solute and porewater transport caused by
563 the presence of an aquaclude-like boundary in the sediment sub-surface (e.g. Tempest et
564 al., 2015) may result in inadequate drainage, stagnant porewater and a lack of aeration. The
565 occurrence of these conditions will inevitably prevent the formation of suitable oxic
566 conditions for re-precipitation of Fe, and Mn, at the sediment surface (Spencer et al., 2008).

567

568 No evidence of an aquaclude was found in either of Cores 2 and 3. In Core 2₁₅, Fe peaked at
569 the terrestrial boundary, corresponding to a peak in loss on ignition values. The increase in
570 residual bulk organic matter, present on the terrestrial surface before site inundation, may
571 well drive bacterially-mediated sulphate reduction following incorporation into the
572 sediment, resulting in the enrichment of Fe via Fe-sulphide formation. No major trends
573 were detected in Fe content through the rest of the sample, where the sediment showed
574 clear red mottling, implying variability in the water table caused by tidal inundation (Cundy
575 and Croudace, 1995). Fe fluctuated through the red mottled Core 3₁₅, indicating a
576 fluctuating water column through the sub-surface sediment.

577

578 Core 2₁₆ was visibly darker in the intertidal and terrestrial facies, decreasing in S and
579 increasing in Fe and Mn to the boundary between the units. The sharp nature of this
580 boundary, and the peak in moisture content may indicate reduced vertical conveyance of
581 water through the unconformity. The fluctuations in Fe, and to a lesser extent Mn, in the
582 pre-reclamation intertidal facies could be caused by trapping authigenic carbonate /
583 sulphide formation (Cundy and Croudace, 1995). In Core 3₁₆, the distribution of Fe
584 continued to indicate a fluctuating water column.

585

586 Broad- and intensive-scale analysis suggests evidence of bacterial reduction of sulphate at
587 the surface of Core 1₁₅ and Core 5₁₅. Below this unit the red mottled sediment and Fe profile
588 implied a variable water column facilitated by the extensive inter-connected macro-pore
589 network indicated by μ CT analysis. An increase in the Fe / Mn ratio in the middle of the

590 sample analysed using high resolution Itrax scanning in Core 5₁₆ suggests redox mobilisation
591 of Mn, which is generally more sensitive to redox changes than Fe. Despite the differences
592 in sediment structure between Core 5 and 6, there was still evidence of Fe enrichment. The
593 macro-pore network was dominated by a large horizontal pore which corresponded to an
594 increase in the intensity of Mn and the Fe / Mn ratio in Itrax data, possibly the result of
595 enrichment via lateral through-flow and indicative that the pore was not an artificial by-
596 product of the sampling procedure. These trends were maintained when re-sampled with
597 no sub-surface unconformity detected in Core 6₁₆. Results presented here differ from the
598 geochemical and redox profiles observed in older MR sites (Spencer et al., 2008), and
599 natural saltmarsh and mudflat environments within the Solent (e.g. Cundy and Croudace,
600 1995). It remains to be seen if the geochemical profiles evolve in a similar manner to other
601 MR sites or towards that of a more typical intertidal setting, compared schematically in the
602 Graphical Abstract, and the timescales required for this development. Not only would this
603 determine the depth of any anoxic layer, which may inhibit biological activity, but will
604 influence nutrient exchange and the partitioning (and possibly release) of contaminants
605 such as metals or pesticides potentially stored within the sediment.

606

607 **6.3 Influence of the Former Land Use and Site Construction**

608

609 MR aims to restore the structure and functioning of intertidal habitats, compensating for
610 losses elsewhere. However, previous studies have demonstrated differences in the physical,
611 geochemical and hydrological characteristics of saltmarshes in MR sites, particularly at the
612 Orplands Farm site (UK), compared to natural marshes (Spencer et al., 2017; Spencer et al.,

613 2008; Tempest et al., 2015). This has resulted in the restoration of intertidal conditions, but
614 not full restoration of the hydrological regime and the physical structure of the intertidal
615 environment which may have consequences for the ecological functioning and ecosystem
616 services provided. It has been proposed that the structural differences between MR and
617 natural sites are the cause of water-logging and poor drainage, which have been attributed
618 to poor saltmarsh species abundance and diversity within MR sites (e.g. Mossman et al.,
619 2012). Clear differences in sediment structure for sites of different former land use were
620 found at the Medmerry Managed Realignment Site. Therefore, it would be anticipated that
621 sites with reduced porosity and pore connectivity would have lower subsurface flow, no or
622 low concentrations of dissolved oxygen, and anoxic sediment. However, analyses of the
623 geochemical profiles at Medmerry do not yet match this expectation.

624

625 Medmerry is still a developing site on the open coast and, therefore, has not experienced a
626 large accretion of intertidal sediment on the former terrestrial land surface, such as
627 observed in older MR sites found in sediment-rich estuarine environments (Spencer et al.,
628 2017; Spencer et al., 2008; Watts et al., 2003; Wolanski and Elliott, 2016). It remains to be
629 seen how the geochemical profiles develop following further accretion of sediment.

630 However, without the accretion of sediment on top of the terrestrial horizon, tidal waters
631 appear to have been able to drain through the terrestrial facies. An exception is the site of
632 Core 2; in the second sample taken from this site sediment appeared black and anoxic, with
633 evidence of water pooling at the terrestrial boundary and reduced hydrological connectivity
634 through the contact between the facies. These findings suggest that hydrological and
635 geochemical differences found in MR sites compared to natural saltmarshes are not caused

636 by sub-surface differences owing to the former land use, but by the formation of an
637 unconformity in the sediment column as a result of (a) the accretion of sediment, and (b)
638 sharp physicochemical contrasts between the accreted upper unit and the underlying
639 sediment. For the latter, in Core 2, it is likely that the formation of an anoxic unit has been
640 driven by the decay of terrestrial vegetation trapped and buried under the accreted
641 sediment following site inundation (French, 2006).

642

643 **7 Conclusion**

644

645 In this paper, differences in the sub-surface structure and physiochemical properties of
646 inundated sites with different former land use histories have been investigated at the
647 Medmerry Managed Realignment Site, during the initial 16 and 36 months after site
648 inundation. A novel combination of repeated broad- and intensive-scale analysis was used
649 to assess differences in the subsurface sediment structure and early geochemical evolution
650 in the three years following site inundation. Results indicate a number of new findings,
651 including:

- 652 • Clear differences are present in the sediment structure and properties at different
653 sites as a result of contrasts in the former land use. Broad-scale analysis suggests
654 sites formerly used more intensively for agricultural purposes have lower moisture
655 content and loss on ignition, with intensive-scale analysis suggesting pore networks
656 were more complex but were less connected and aligned at these sites.

657 • Evidence of reduced drainage and anoxic conditions, identified in previous studies
658 (e.g. Spencer et al., 2017; Tempest et al., 2015) as a result of modifications caused by
659 a site's terrestrial history, were not found at Medmerry except at the site which had
660 experienced the highest level of accretion (*ca.* 7 cm in 36 months).

661

662 Further work is now required to assess if the differences in sediment structure, identified in
663 this study, can be detected in other (including older) MR sites where greater levels of post-
664 site inundation accumulation have occurred. The findings in this study indicate that the
665 formation of an aquaclude, reducing vertical solute transfer between facies, is not a direct
666 consequence of changes to the sediment caused by the former land use, but is the result of
667 the accretion of sediment, coupled with sharp physicochemical contrasts between the
668 accreted upper layer and the underlying sediment. Many MR sites are designed to
669 accumulate sediment, but these findings highlight the need for improved awareness of
670 sediment accretion in decision-making in the design of MR sites, alongside hydrodynamic
671 and topographic considerations. While further work on other MR sites is needed to assess
672 how widespread this accretionary effect is, the data presented here indicate that sites need
673 to be designed to encourage rapid accumulation of intertidal sediment, burying the
674 terrestrial boundary and so minimising the effect of an aquaclude. Alternatively, predictions
675 need to be adjusted to anticipate reduced saltmarsh diversity abundance, and therefore
676 ecosystem services delivery, until sufficient sediment has been accreted.

677

678

679 **Acknowledgements**

680

681 The authors would like to thank the two anonymous reviewers for their comments, which
682 have helped improve the manuscript. The authors would also like to thank: Matthew Leake
683 (University of Brighton) for his assistance during field work, Magda Grove, Peter Lyons (both
684 University of Brighton) and Lucy Diggins (Queen Mary University of London) for their
685 assistance with laboratory analysis, Callum Firth for his support and guidance during JD's
686 studentship and during fieldwork. X-ray microtomography was carried out by the School of
687 Geography, Queen Mary University of London. The authors are grateful to the BOSCORF
688 facility at the National Oceanography Centre (Southampton) for access to Itrax facilities.
689 Research was funded by the Environment Agency (United Kingdom).

690

691

692 **References**

- 693 Auxtero E, Shamshuddin J, Paramanathan S. Mineralogy, morphology and classification of
694 acid sulfate soils in Pulau Lumut, Selangor. *Pertanika* 1991; 14: 43-51.
- 695 Bergen SD, Bolton SM, L. Fridley J. Design principles for ecological engineering. *Ecological*
696 *Engineering* 2001; 18: 201-210.
- 697 Berrow ML, Stein WM. Extraction of metals from soils and sewage sludges by refluxing with
698 aqua regia. *Analyst* 1983; 108: 277-285.
- 699 Beven K, Germann P. Macropores and water flow in soils revisited. *Water Resources*
700 *Research* 2013; 49: 3071-3092.
- 701 Bone AE. The shaping of the Selsey coastline: a review of the geomorphology, archaeology
702 and history. *Tertiary Research* 1996; 16: 5-14.
- 703 Burton ED, Bush RT, Johnston SG, Sullivan LA, Keene AF. Sulfur biogeochemical cycling and
704 novel Fe-S mineralization pathways in a tidally re-flooded wetland. *Geochimica Et*
705 *Cosmochimica Acta* 2011; 75: 3434-3451.
- 706 Cnudde V, Boone MN. High-resolution X-ray computed tomography in geosciences: A review
707 of the current technology and applications. *Earth-Science Reviews* 2013; 123: 1-17.
- 708 Cochran JK, Hirschberg DJ, Wang J, Dere C. Atmospheric deposition of metals to coastal
709 waters (Long Island Sound, New York USA): Evidence from saltmarsh deposits.
710 *Estuarine Coastal and Shelf Science* 1998; 46: 503-522.
- 711 Cope S, Bradbury A, Gorczynska M. Solent Dynamic Coast Project: Main Report; A tool for
712 SMP2, New Forest District Council/Channel Coastal Observatory, 2008.
- 713 Costanza R, d'Arge R, deGroot R, Farber S, Grasso M, Hannon B, et al. The value of the
714 world's ecosystem services and natural capital. *Nature* 1997; 387: 253-260.
- 715 Crooks S, Pye K. Sedimentological controls on the erosion and morphology of saltmarshes:
716 implications for flood defence and habitat recreation. In: Pye K, Allen JRL, editors.
717 *Coastal and Estuarine Environments: Sedimentology, Geomorphology and*
718 *Geoarchaeology*. 175, 2000, pp. 207-222.
- 719 Crooks S, Schutten J, Sheern GD, Pye K, Davy AJ. Drainage and elevation as factors in the
720 restoration of salt marsh in Britain. *Restoration Ecology* 2002; 10: 591-602.
- 721 Croudace IW, Rindby A, Rothwell RG. ITRAX: description and evaluation of a new multi-
722 function X-ray core scanner. Geological Society, London, Special Publications 2006;
723 267: 51-63.
- 724 Cundy AB, Croudace IW. Sedimentary and geochemical variations in a salt-marsh mud flat
725 environment from the mesotidal Hamble estuary, southern England. *Marine*
726 *Chemistry* 1995; 51: 115-132.
- 727 Cundy AB, Kortekaas S, Dewez T, Stewart IS, Collins PEF, Croudace IW, et al. Coastal
728 wetlands as recorders of earthquake subsidence in the Aegean: a case study of the
729 1894 Gulf of Atalanti earthquakes, central Greece. *Marine Geology* 2000; 170: 3-26.
- 730 Cundy AB, Long AJ, Hill CT, Spencer C, Croudace IW. Sedimentary response of Pagham
731 Harbour, southern England to barrier breaching in AD 1910. *Geomorphology* 2002;
732 46: 163-176.
- 733 Cundy AB, Sprague D, Hopkinson L, Maroukian H, Gaki-Papanastassiou K, Papanastassiou D,
734 et al. Geochemical and stratigraphic indicators of late Holocene coastal evolution in
735 the Gythio area, southern Peloponnese, Greece. *Marine Geology* 2006; 230: 161-
736 177.

737 Dale J, Burgess HM, Burnside NG, Kilkie P, Nash DJ, Cundy AB. The evolution of embryonic
738 creek systems in a recently inundated large open coast managed realignment site.
739 *Anthropocene Coasts* 2018a; 1: 16-33.

740 Dale J, Burgess HM, Cundy AB. Sedimentation rhythms and hydrodynamics in two
741 engineered environments in an open coast managed realignment site. *Marine*
742 *Geology* 2017; 383: 120-131.

743 Dale J, Burgess HM, Nash DJ, Cundy AB. Hydrodynamics and sedimentary processes in the
744 main drainage channel of a large open coast managed realignment site. *Estuarine,*
745 *Coastal and Shelf Science* 2018b.

746 Davy AJ, Brown MJH, Mossman HL, Grant A. Colonization of a newly developing salt marsh:
747 disentangling independent effects of elevation and redox potential on halophytes.
748 *Journal of Ecology* 2011; 99: 1350-1357.

749 Doherty JM, Callaway JC, Zedler JB. Diversity-function relationships changed in a long-term
750 restoration experiment. *Ecological Applications* 2011; 21: 2143-2155.

751 Doody JP. 'Coastal squeeze' - an historical perspective. *Journal of Coastal Conservation*
752 2004; 10: 129-138.

753 Elliott M, Mander L, Mazik K, Simenstad C, Valesini F, Whitfield A, et al. Ecoengineering with
754 Ecohydrology: Successes and failures in estuarine restoration. *Estuarine, Coastal and*
755 *Shelf Science* 2016; 176: 12-35.

756 Environment Agency. Pagham to East Head Coastal Defence Strategy, Worthing, 2007.

757 Erfanzadeh R, Garbutt A, Petillon J, Maelfait JP, Hoffmann M. Factors affecting the success
758 of early salt-marsh colonizers: seed availability rather than site suitability and
759 dispersal traits. *Plant Ecology* 2010; 206: 335-347.

760 Esteves LS. Is managed realignment a sustainable long-term coastal management approach?
761 *Journal of Coastal Research* 2013; Special Issue 65: 933-938.

762 European Parliament and the Council of the European Commission. Council directive
763 92/43/EEC of 21 May 1992 on the conservation of natural habitats and of wild fauna
764 and flora. *Official Journal of the European Communities* 1992; Series L206:
765 22.12.2000.

766 Foster NM, Hudson MD, Bray S, Nicholls RJ. Research, policy and practice for the
767 conservation and sustainable use of intertidal mudflats and saltmarshes in the Solent
768 from 1800 to 2016. *Environmental Science & Policy* 2014; 38: 59-71.

769 French PW. Managed realignment - The developing story of a comparatively new approach
770 to soft engineering. *Estuarine Coastal and Shelf Science* 2006; 67: 409-423.

771 Hazelden J, Boorman LA. Soils and 'managed retreat' in South East England. *Soil Use and*
772 *Management* 2001; 17: 150-154.

773 Howe AJ, Rodriguez JF, Spencer J, MacFarlane GR, Saintilan N. Response of estuarine
774 wetlands to reinstatement of tidal flows. *Marine and Freshwater Research* 2010; 61:
775 702-713.

776 Hvorslev MJ. Subsurface exploration and sampling of soils for civil engineering purposes.
777 Vicksburg, Mississippi: Waterways Experiment Station, 1949.

778 Johnston SG, Keene AF, Bush RT, Burton ED, Sullivan LA, Isaacson L, et al. Iron geochemical
779 zonation in a tidally inundated acid sulfate soil wetland. *Chemical Geology* 2011;
780 280: 257-270.

781 Ketcham RA, Carlson WD. Acquisition, optimization and interpretation of X-ray computed
782 tomographic imagery: applications to the geosciences. *Computers & Geosciences*
783 2001; 27: 381-400.

784 Koretsky CM, Van Cappellen P, DiChristina TJ, Kostka JE, Lowe KL, Moore CM, et al. Salt
785 marsh pore water geochemistry does not correlate with microbial community
786 structure. *Estuarine, Coastal and Shelf Science* 2005; 62: 233-251.

787 Krawiec K. Medmerry, West Sussex, UK: Coastal Evolution from the Neolithic to the
788 Medieval Period and Community Resilience to Environmental Change. *The Historic
789 Environment: Policy & Practice* 2017; 8: 101-112.

790 Luther GW, Church TM. Seasonal cycling of sulfur and iron in porewaters of a Delaware salt-
791 marsh. *Marine Chemistry* 1988; 23: 295-309.

792 Marani M, Silvestri S, Belluco E, Ursino N, Comerlati A, Tosatto O, et al. Spatial organization
793 and ecohydrological interactions in oxygen-limited vegetation ecosystems. *Water
794 Resources Research* 2006; 42.

795 Mazik K, Musk W, Dawes O, Solyanko K, Brown S, Mander L, et al. Managed realignment as
796 compensation for the loss of intertidal mudflat: A short term solution to a long term
797 problem? *Estuarine, Coastal and Shelf Science* 2010; 90: 11-20.

798 Miller H, Croudace IW, Bull JM, Cotterill CJ, Dix JK, Taylor RN. A 500 Year Sediment Lake
799 Record of Anthropogenic and Natural Inputs to Windermere (English Lake District)
800 Using Double-Spike Lead Isotopes, Radiochronology, and Sediment Microanalysis.
801 *Environmental Science & Technology* 2014; 48: 7254-7263.

802 Moller I, Kudella M, Rupprecht F, Spencer T, Paul M, van Wesenbeeck BK, et al. Wave
803 attenuation over coastal salt marshes under storm surge conditions. *Nature
804 Geoscience* 2014; 7: 727-731.

805 Mossman HL, Brown MJH, Davy AJ, Grant A. Constraints on Salt Marsh Development
806 Following Managed Coastal Realignment: Dispersal Limitation or Environmental
807 Tolerance? *Restoration Ecology* 2012; 20: 65-75.

808 Odgaard A. Three-dimensional methods for quantification of cancellous bone architecture.
809 *Bone* 1997; 20: 315-328.

810 Pearce J, Khan S, Lewis P. Medmerry managed realignment—sustainable coastal
811 management to gain multiple benefits. *ICE Coastal Management. Innovative Coastal
812 Zone Management: Sustainable Engineering for a Dynamic Coast.*, Belfast, UK, 2011.

813 Polder G, Hovens H, Zweers A. Measuring shoot length of submerged aquatic plants using
814 graph analysis. *Proceedings of the ImageJ User and Developer Conference 2010,
815 Mondorf-les-Bains, Luxembourg, 27-29 October 2010, 2010, pp. 172-177.*

816 Reid MK, Spencer KL. Use of principal components analysis (PCA) on estuarine sediment
817 datasets: The effect of data pre-treatment. *Environmental Pollution* 2009; 157:
818 2275-2281.

819 Rowell DL. *Soil science: Methods & applications.* Harlow, Essex: Longman Scientific &
820 Technical, 1994.

821 Rupprecht F, Moller I, Paul M, Kudella M, Spencer T, van Wesenbeeck BK, et al. Vegetation-
822 wave interactions in salt marshes under storm surge conditions. *Ecological
823 Engineering* 2017; 100: 301-315.

824 Shennan I, Long AJ, Rutherford MM, Green FM, Innes JB, Lloyd JM, et al. Tidal marsh
825 stratigraphy, sea-level change and large earthquakes, i: a 5000 year record in
826 washington, U.S.A. *Quaternary Science Reviews* 1996; 15: 1023-1059.

827 Shennan I, Long AJ, Rutherford MM, Innes JB, Green FM, Walker KJ. Tidal marsh
828 stratigraphy, sea-level change and large earthquakes—ii: Submergence events
829 during the last 3500 years at Netarts Bay, Oregon, USA. *Quaternary Science Reviews*
830 1998; 17: 365-393.

831 Spencer KL, Carr SJ, Diggens LM, Tempest JA, Morris MA, Harvey GL. The impact of pre-
832 restoration land-use and disturbance on sediment structure, hydrology and the
833 sediment geochemical environment in restored saltmarshes. *Science of The Total*
834 *Environment* 2017; 587–588: 47-58.

835 Spencer KL, Cundy AB, Croudace IW. Heavy metal distribution and early-diagenesis in salt
836 marsh sediments from the Medway Estuary, Kent, UK. *Estuarine Coastal and Shelf*
837 *Science* 2003; 57: 43-54.

838 Spencer KL, Cundy AB, Davies-Hearn S, Hughes R, Turner S, MacLeod CL. Physicochemical
839 changes in sediments at Orplands Farm, Essex, UK following 8 years of managed
840 realignment. *Estuarine Coastal and Shelf Science* 2008; 76: 608-619.

841 Tempest JA, Harvey GL, Spencer KL. Modified sediments and subsurface hydrology in natural
842 and recreated salt marshes and implications for delivery of ecosystem services.
843 *Hydrological Processes* 2015; 29: 2346-2357.

844 Violante A, Barberis E, Pigna M, Boero V. Factors affecting the formation, nature, and
845 properties of iron precipitation products at the soil-root interface. *Journal of Plant*
846 *Nutrition* 2003; 26: 1889-1908.

847 Vogel HJ. Morphological determination of pore connectivity as a function of pore size using
848 serial sections. *European Journal of Soil Science* 1997; 48: 365-377.

849 Vranken M, Oenema O, Mulder J. Effects of tide range alterations on salt-marsh sediments
850 in the eastern Scheldt, SW Netherlands. *Hydrobiologia* 1990; 195: 13-20.

851 Watts CW, Tolhurst TJ, Black KS, Whitmore AP. In situ measurements of erosion shear stress
852 and geotechnical shear strength of the intertidal sediments of the experimental
853 managed realignment scheme at Tollesbury, Essex, UK. *Estuarine Coastal and Shelf*
854 *Science* 2003; 58: 611-620.

855 Wilson AM, Evans T, Moore W, Schutte CA, Joye SB, Hughes AH, et al. Groundwater controls
856 ecological zonation of salt marsh macrophytes. *Ecology* 2015; 96: 840-849.

857 Wolanski E, Elliott M. *Estuarine Ecohydrology (Second Edition)*. Boston: Elsevier, 2016.

858 Zwolsman JJG, Berger GW, Vaneck GTM. Sediment accumulation rates, historical input,
859 postdepositional mobility and retention of major elements and trace-metals in salt-
860 marsh sediments of the Scheldt estuary, SW Netherlands. *Marine Chemistry* 1993;
861 44: 73-94.

862

863

864

**Medmerry Managed
Realignment Site
(West Sussex, United
Kingdom)**

**Orplands Farm Managed
Realignment Site (Essex,
United Kingdom)**

**Natural Saltmarsh
(Hamble estuary,
Hampshire,
United Kingdom)**

<p>Post-site inundation intertidal</p>	<p>Physical properties varied in</p>	<p>Post-site inundation: Poorly consolidated oxic unit with a high abundant root material and omxplex, interconnected pore networks</p>	<p>Layer 1: Thin (mm) oxidised surface layer rich in plant litter</p>
<p>Terrestrial</p>	<p>terrestrial unit but mottled oxic conditions were found throughout suggesting a variable</p>	<p>Terrestrial: Firmer sediment layer, lower in organic and moisture content. Geochemical (lower Fe and Mn concentrations), structural (reduced pore distribution and complexity) and</p>	<p>Layer 2: Mottled oxic zone with evidence of a fluctuating water table, rich in abundant (living) root material</p>
<p>Pre- reclamation intertidal</p>	<p>water table and that vertical solute transfer is not inhibited</p>	<p>hydrological (reduced vertical water flux) evidences suggests reduced solute transfer between units</p>	<p>Layer 3: Black unit with reducing anoxic conditions, increased water content</p>

Graphical Abstract: Schematic comparison of the sub-surface physicochemical properties of the sediment found at the Medmerry Managed Realignment Site (this study), Orplands Farm Managed Realignment Site, U.K. (Spencer et al., 2008; Tempest et al., 2015; Spencer et al., 2017) and a typical natural minerogenic saltmarsh (Cundy and Croudace, 1995). Not drawn to uniform vertical scale.

Figures

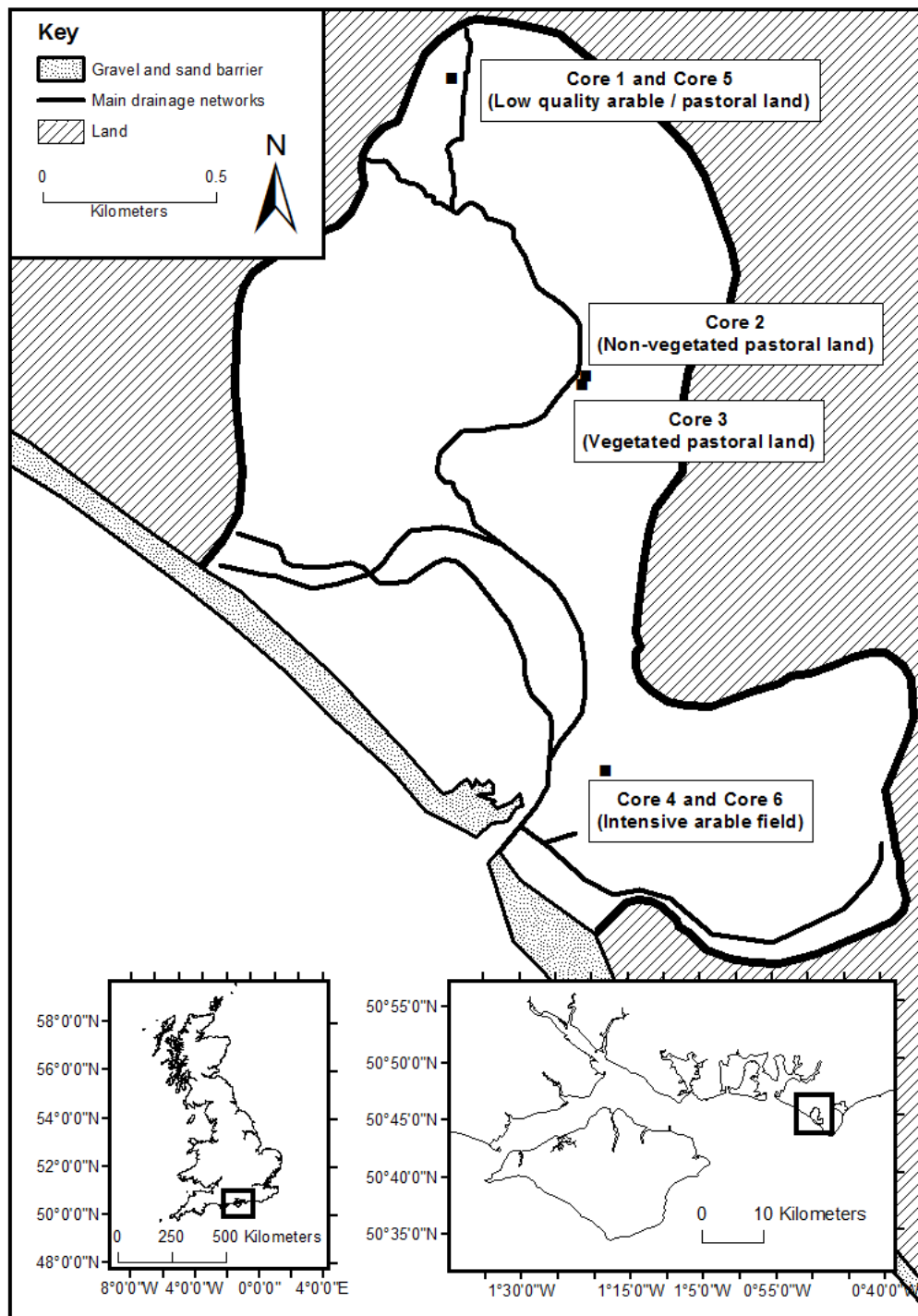


Figure 1: The Medmerry Managed Realignment Site (West Sussex, UK) and wider national (insert, left) and regional (insert, right) location. Coring locations are named and marked with black squares.

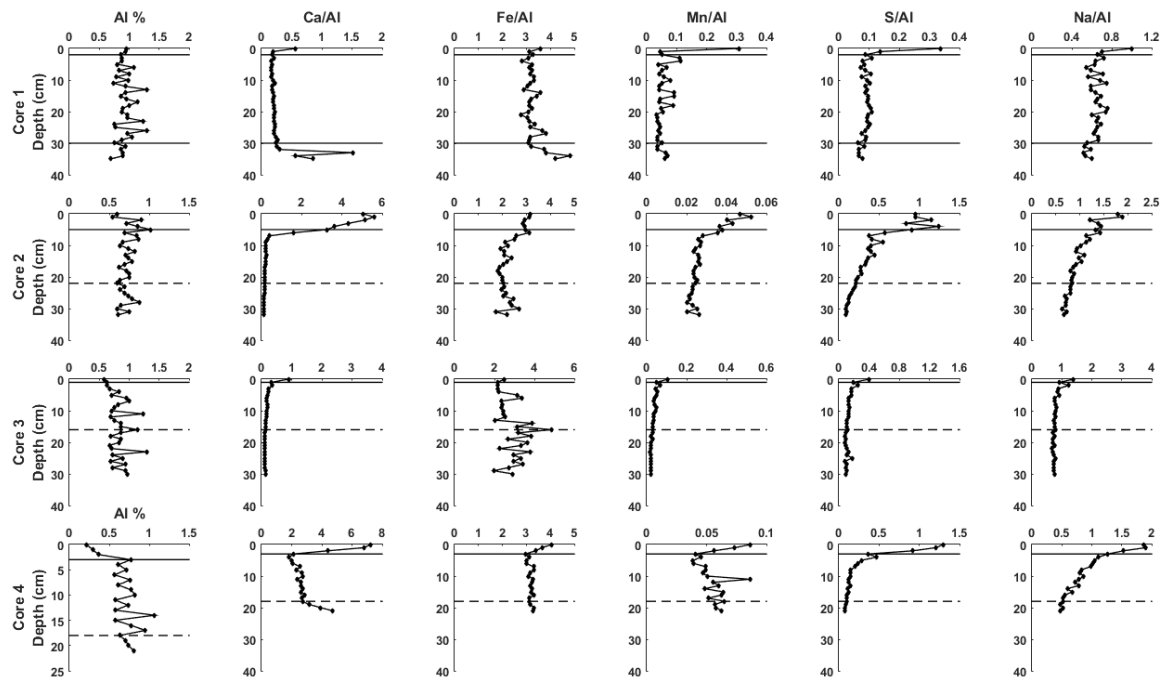


Figure 2: Variations in Al, Ca, Fe, Mn, S and Na concentration with depth from the 2015 core samples.

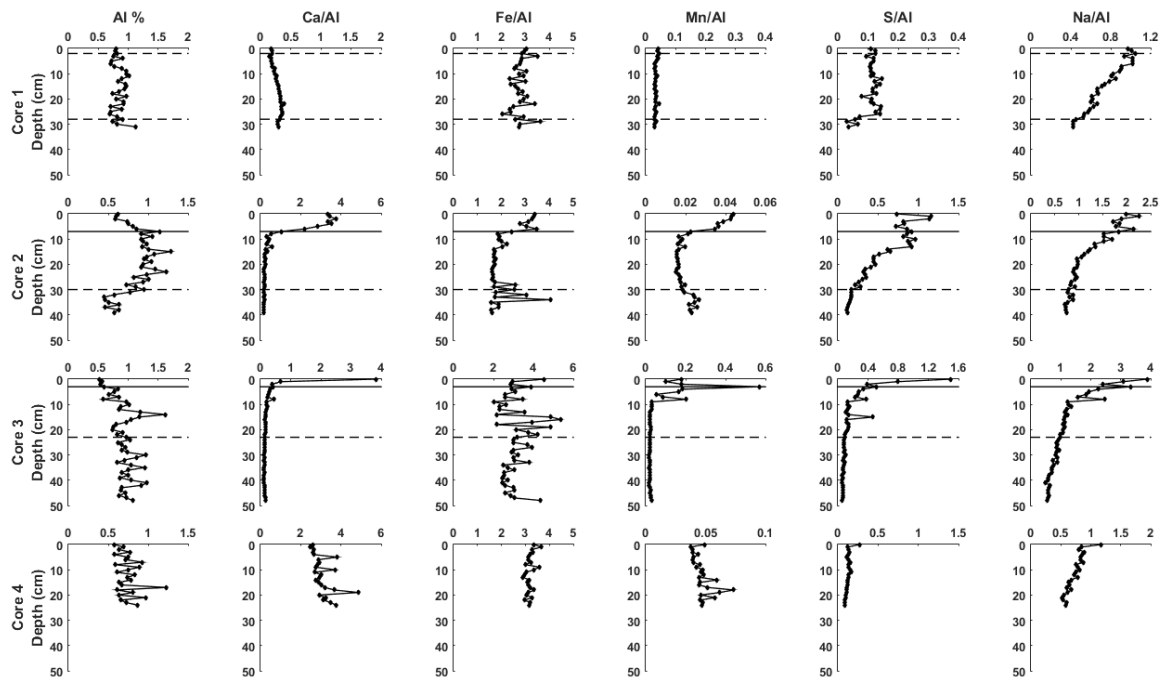


Figure 3: Variations in Al, Ca, Fe, Mn, S and Na concentration with depth from the 2016 core samples.

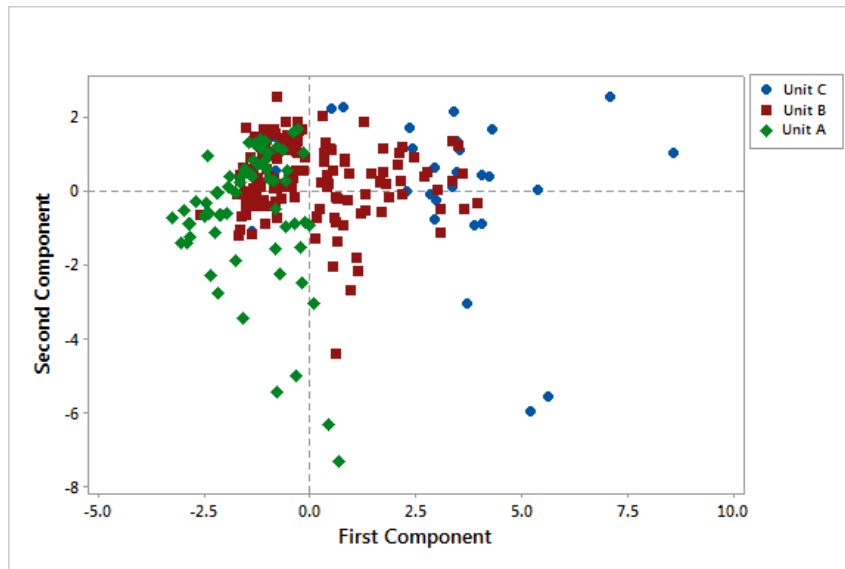


Figure 4: Principle component analysis (PCA) scores for the three sediment units identified in Cores 1 – 4 in 2015 and Cores 1 – 3 in 2016. Components 1 and 2 collectively accounted for 49.6 % of the total variance.

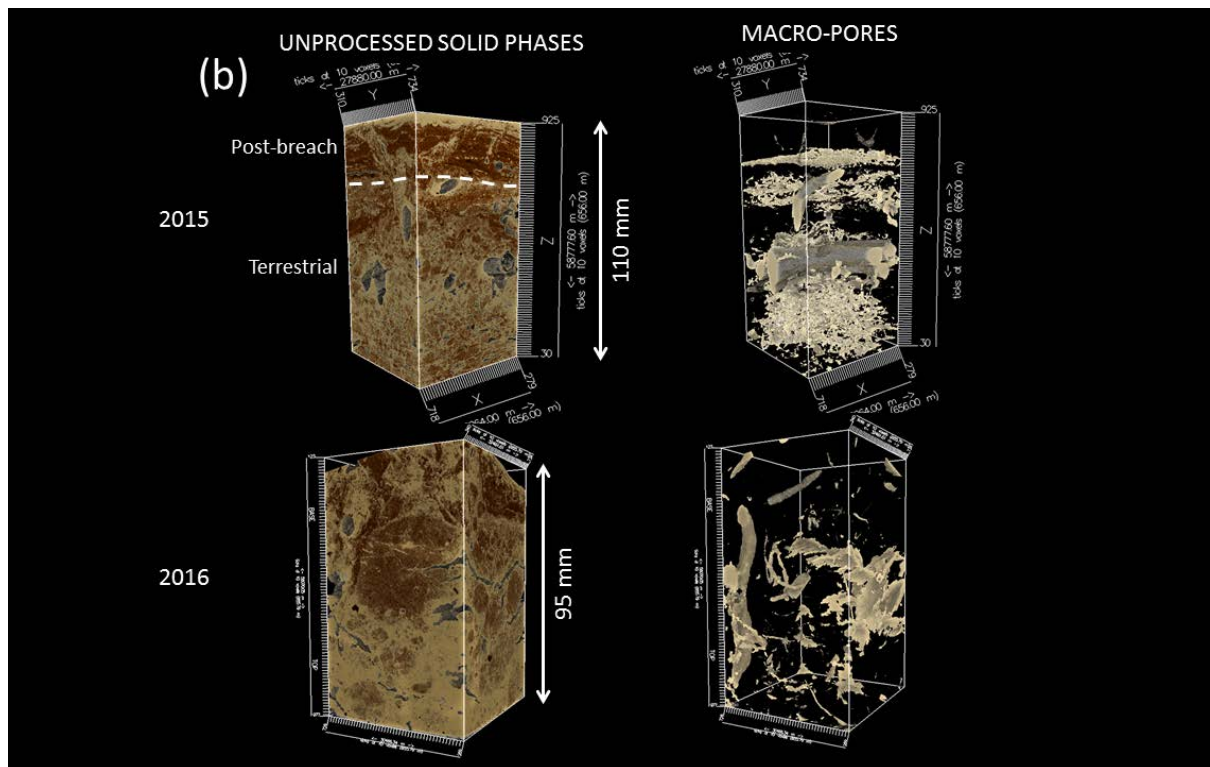
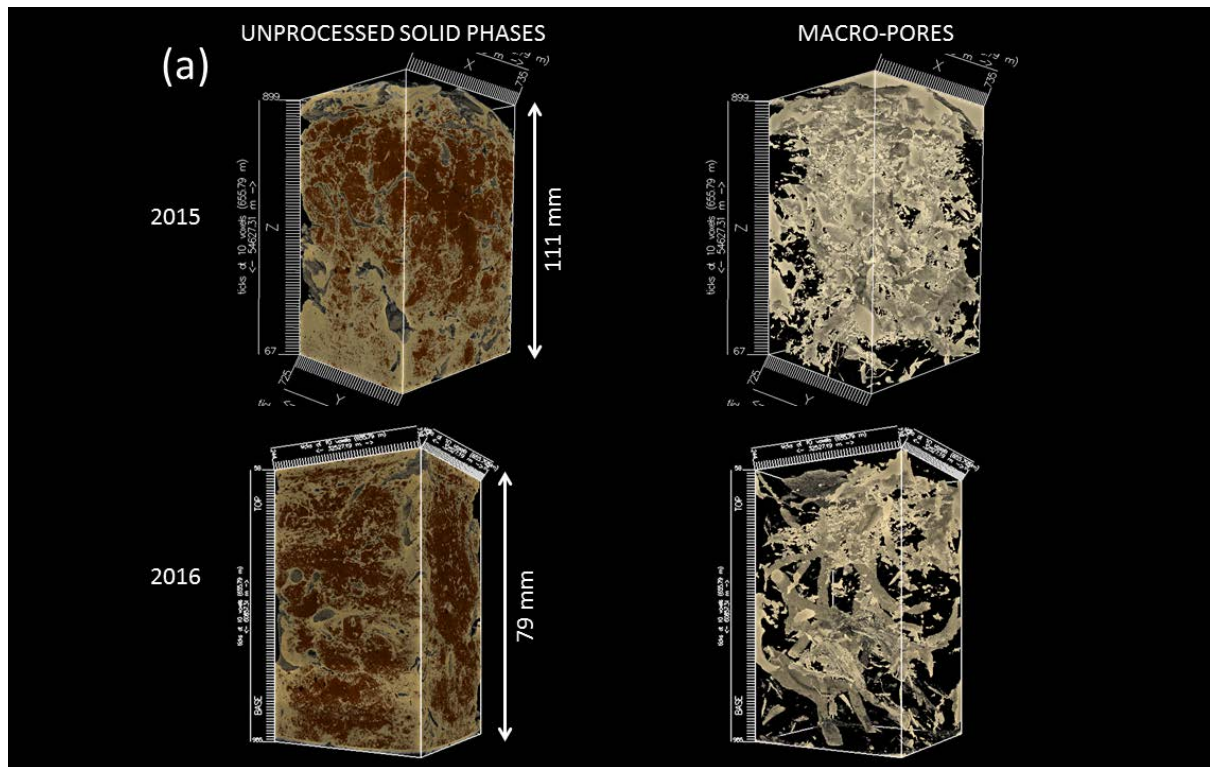


Figure 5: Reconstructions of sediment phases imaged used μ CT analysis in (a) Core 1 and (b) Core 2.

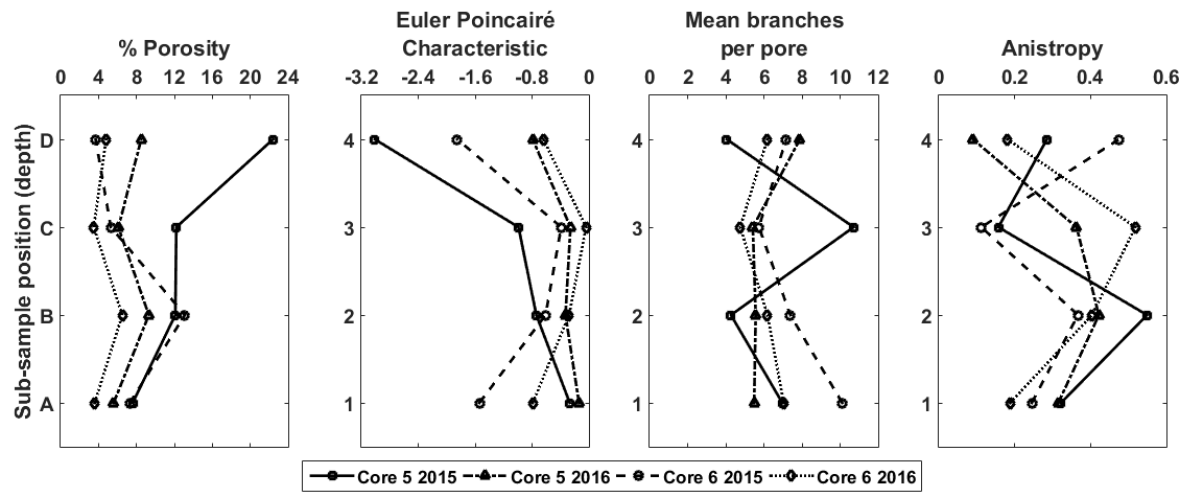
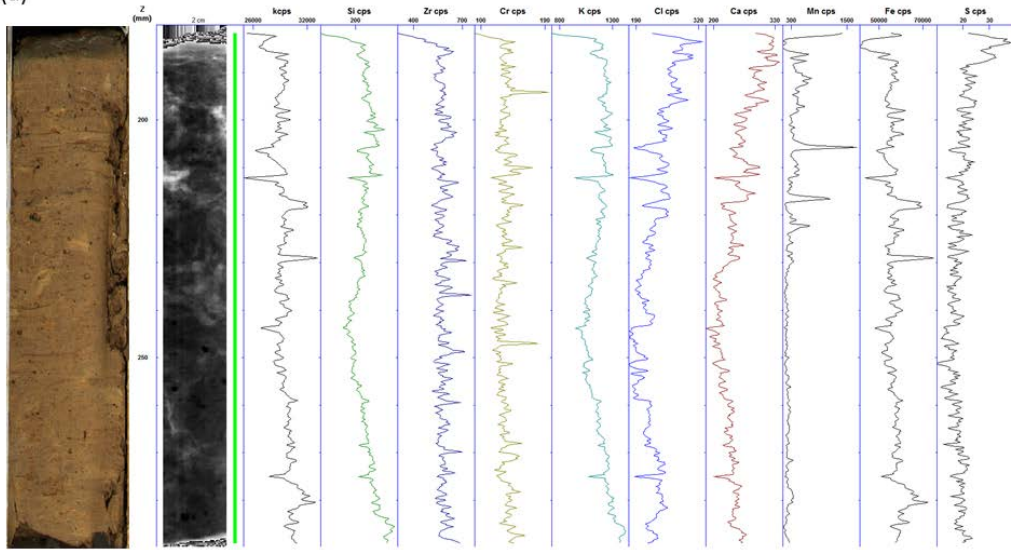
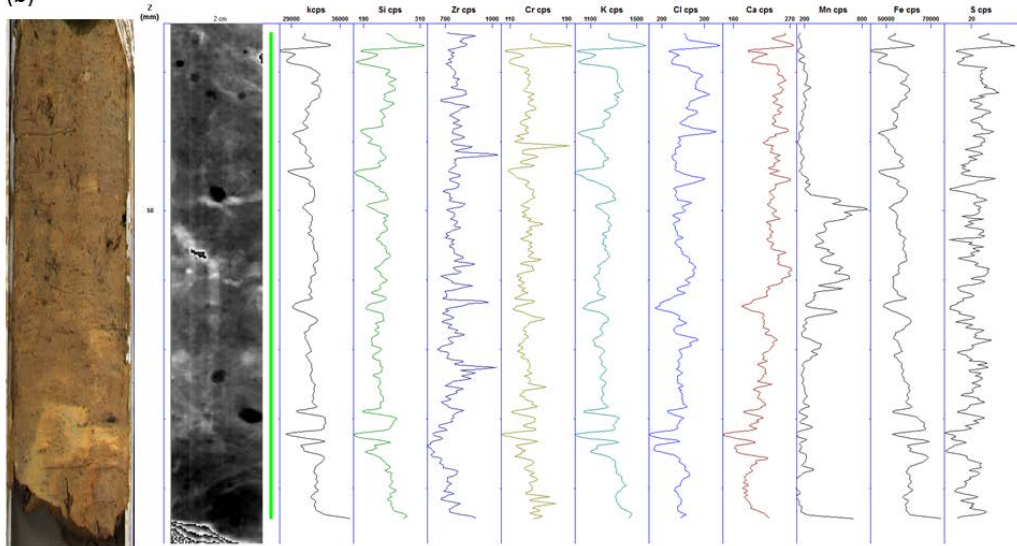


Figure 6: Porosity characteristics for sub-samples of Cores 5 and 6 in 2016 and 2017.

(a)



(b)



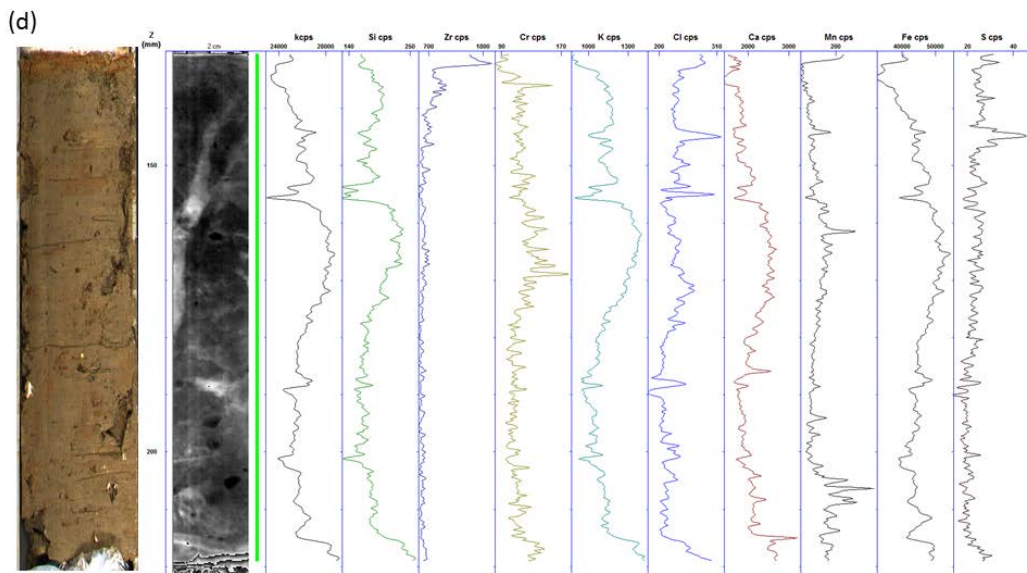
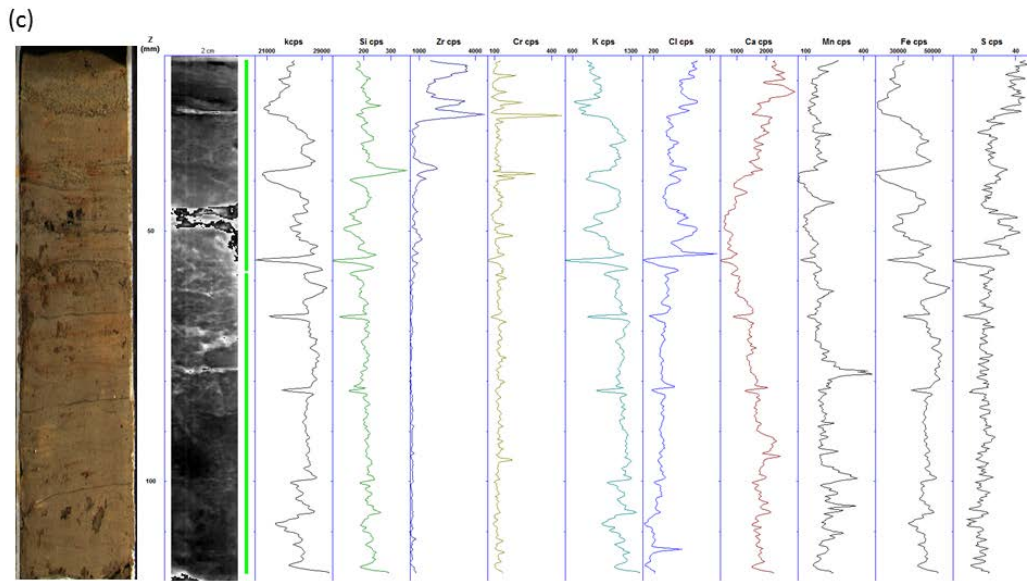


Figure 7: Si, Zr, Cr, K, Cl, Ca, Mn, Fe and S distribution, X-radiograph and photograph of core from (a) Core 5₁₅, (b) Core 5₁₆, (c) Core 6₁₅ and (d) Core 6₁₆. Data are from Itrax scanning: X-axis shows X-ray response, y-axis represents depth.

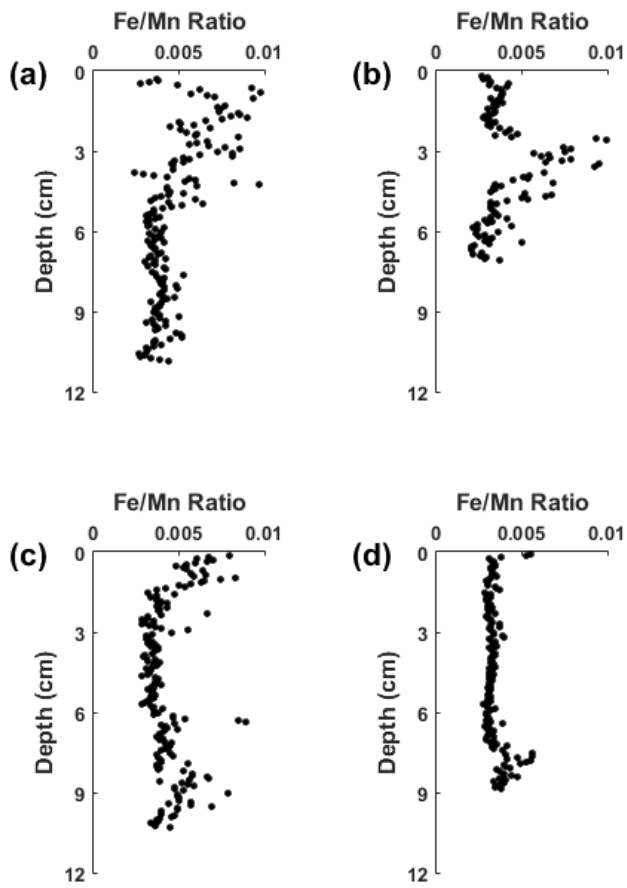


Figure 8: Fe / Mn ratio for (a) Core 5₁₅, (b) Core 5₁₆, (c) Core 6₁₅ and (d) Core 6₁₆ derived from Itrax geochemical data.

Tables

Table 1: Former (terrestrial) land use at sampling locations within the Medmerry Managed Realignment Site and the proposed structural state.

Site	Terrestrial Land Use	Proposed Structure and Composition
Core 1	Low quality arable / pastoral land	Some compaction but interconnected pore networks still expected to be present
Core 2	Non-vegetated pastoral land	Uncompact freely draining sediment
Core 3	Vegetated pastoral land	
Core 4	Intensive arable field	Compact, with low abundance of pore networks resulting lower subsurface solute transfer and anoxic conditions

Table 2: Mean values for physical sediment characteristics for the three sediment units identified (see text for discussion) at the four coring sites (see Figure 1 for locations) in 2015 and 2016.

		Wet Bulk Density (kg m ⁻³)		Moisture Content (%)		Porosity		Loss on Ignition (%)		Median Grain Size (µm)		Mud (clay + silt) Content (%)		
		Mean	SD	Mean	SD	Mean	SD	Mean	SD	Mean	SD	Mean	SD	
		Core 1	2015	Unit C	0.76	0.2	62.22	22.14	0.68	0.11	7.58	0.59	6.58	0.58
Unit B	0.86			0.16	49.04	3.59	0.62	0.07	6.95	2.9	8.44	1.58	94.12	2.52
Unit A	0.89			0.16	43.99	9.05	0.58	0.09	7.51	2.16	15.34	3.76	92.23	2.95
2016	Unit C		1.94	0.34	44.82	0.78	0.5	0.09	6.79	11.33	6.03	1.88	89.83	9.77
	Unit B		1.88	0.22	46.42	3.49	0.52	0.06	6.16	5.49	6.71	1.05	87.28	5.25
	Unit A		2.08	0.35	41.84	4.86	0.44	0.11	4.07	3.74	6.19	0.41	91.2	1.45
Core 2	2015	Unit C	0.92	0.23	123.08	14.49	0.72	0.07	5.73	1.83	7.47	0.4	97.67	2.26
		Unit B	1.02	0.38	96.23	21.28	0.65	0.13	9.92	5.87	15.68	8.61	81.44	11.15
		Unit A	1.51	0.45	48.8	6.2	0.33	0.19	7.01	4.72	16.91	5.65	79.48	7.83
	2016	Unit C	1.48	0.27	100.92	5.59	0.72	0.05	4.96	6.15	10.05	2.04	77.36	6.76
		Unit B	1.39	0.33	97.37	29.84	0.73	0.09	12.48	8.54	11.51	7.96	68.23	9.39
		Unit A	1.75	0.3	40.69	8.3	0.53	0.1	4.83	11.1	33.15	25.68	54.1	14.62
Core 3	2015	Unit C	0.64	0.06	122.21	9.46	0.81	0.02	18.61	0.47	6.42	0.78	96.19	3.32
		Unit B	0.99	0.28	69.34	11.05	0.61	0.12	13.48	2.77	6.7	0.77	95.18	2.62
		Unit A	0.93	0.2	51.46	12.19	0.58	0.1	4.52	3.74	5.46	0.59	96.79	5.63
	2016	Unit C	1.39	0.21	118.04	26.02	0.76	0.03	19.21	3.65	11.06	0.86	73.86	3.16
		Unit B	1.71	0.28	69.06	17.39	0.61	0.09	9.88	6.89	7.46	2.46	84.49	7.96
		Unit A	2.18	0.28	40.66	3.64	0.41	0.08	3.24	8.7	7.39	3.25	84.81	9.4
Core 4	2015	Unit C	0.94	0.14	47.95	0.67	0.58	0.07	5.5	15.66	46.48	28.77	59.17	20.19
		Unit B	0.98	0.2	42.25	3.7	0.54	0.1	5.18	3.83	8.54	1.48	89.73	5.13
		Unit A	0.93	0.14	36.89	1.97	0.55	0.07	4.38	1.44	7.52	0.6	92.29	2.33
	2016	Unit A	1.94	0.33	36.62	4.4	0.46	0.09	4.85	8.59	10.2	8.43	78.06	9.93

Table 3: Porosity analysis derived from μ CT analysis divided into sub-samples. Data are presented based on different sediment facies. Core 5 was taken from an area of former lower intensity arable agriculture; Core 6 was taken from an area of former high intensity arable agriculture.

	% Macroporosity	Macro-pore abundance	Pore Connectivity (Euler-Poincaré Characteristic)	Pore network complexity (no. of braches per pore)	Pore Anisotropy
Core 5 2015 A-D	7.6 – 22.4	Low (mean 3672), particularly in the upper sub-sample	-3.01 – -0.27, increasing upwards apart from upper sub-sample	4.05 – 10.71 with no distinctive patterns evident	Moderately high (mean 0.33), although much higher in lower (A and B) sub-samples
Core 5 2016 A-D	5.6 – 6.1	High (mean 5265) although lower in the upper sub- sample	-0.79 – -0.14, increasing upwards apart from upper sub-sample	5.42 – 7.89. Higher in upper sub- sample compared to other three	Moderately high (mean 0.3), but particularly low in upper sub- sample
Core 6 2015 lower facies A- C	5.3 – 13.1	High (mean 5133) and decreasing with depth	-1.54 – 0.39, increasing upwards apart from upper sub-sample	5.74 – 10.11, decreasing upwards.	Moderately low (mean 0.24)
Core 6 2015 upper facies D (post- breach)		3.7 Very high (9458)		7.17, greater than the preceding sub- sample	High (0.48)
Core 6 2016 A-D	3.5 – 6.5	Moderately high (mean 4608) and decreasing downwards	-0.79 – -0.04, increasing upwards apart from upper sub-sample	4.76 – 7.04, following same pattern as 2015 sample.	Moderately high (mean 0.32), although lower in upper and lower sub-samples (A and D)